Growth of Bismuth Sulfide Nanowire Using Bismuth Trisxanthate Single Source Precursors

Yee Wee Koh,[†] Chian Sing Lai,[†] An Yan Du,[‡] Edward R. T. Tiekink,*[,†] and Kian Ping Loh*[,†]

Department of Chemistry, National University of Singapore, 3 Science Drive 3, Singapore 117543, and Institute of Microelectronics, 11 Science Park Road, Singapore Science Park II, Singapore 117685

Received December 20, 2002. Revised Manuscript Received July 18, 2003

Crystalline Bi_2S_3 nanorods, nanotapes, and nanocrystals were obtained from the solvent thermalysis of bismuth trisxanthate precursors and related bismuth dithiocarbamate species in ethylene glycol at 197 °C. Precursors with different structural motifs were designed to produce compounds with different thermal decomposition temparatures, i.e., the dimeric motif of $Bi(S_2COR)_3$ when R = methyl and ethyl was found to have a lower decomposition temperature compared to precursors adopting the polymeric structure, so that solvothermalysis of the former gave rise to short nanocrystals; while in the case of the latter, long nanofibers were produced instead. Chemical vapor deposition on silicon substrates yielded well-defined nanorods of various lengths and diameters for almost all precursors. Internal microstructure of the nanorods was studied by high-resolution transmission electron microscopy.

1. Introduction

The growth and electrical characterization of nanocrystalline semiconductors with lamellar structures, for example Bi_2S_3, is of considerable current interest. To a first approximation, the structure of Bi_2S_3 comprises a macromolecular lamellar net with trigonally coordinated Bi and S atoms. The Bi_2S_3 layers are connected via weaker intermolecular Bi···S bonds, with this being a unique feature of the material that can give rise to potential nanostructures under certain growth conditions. Thus, the exfoliation of the crystal structure along the weak intermolecular bonds, or the rapid growth of the crystal along the *c*-axis may give rise to dimensional structures such as nanosheets or nanofibers. Owing to the anisotropic nature of structures such as Bi_2S_3, layers of lamellar semiconductors may be regarded as colloidal analogues of quantum well structures.[1,2] Quantum size effects have been reported by Variano et al.[3] for disklike particles of Bi_2S_3 prepared in microemulsions, for which the anisotropic particle-in-a-box model has been applied. Compared to nanocrystals of II/VI semiconductors in which quantum confinement occurs in a three-dimensional box, the charge carriers in anisotropic lamellar nanostructures are confined in the 1- or 2-dimensional realm.

Macrocrystalline thin films of Bi_2S_3 have been used in electronic devices such as photodiode arrays[4−6] as its forbidden gap lies between 1.25 and 1.7 eV.[7−10] By contrast, noncrystalline Bi_2S_3 films were found to cause significant changes in photoelectrochemical cell performance because of their quantum size effects.[11] Given the use and potential applications of Bi_2S_3, the challenge is to generate high purity Bi_2S_3 in both an economical and reliable fashion. Previous approaches for the synthesis of Bi_2S_3 thin films include chemical bath and electrospray synthesis methods with the use of different sulfide releasing sources such as thiosulfate, thiourea, and thioacetamide.[12−17]

There have been several reports recently on the use of single-source precursors, containing bismuth and sulfur within the one molecule, for the growth of Bi_2S_3

* Authors to whom correspondence should be addressed. Loh Kian Ping E-mail: chmlohkp@nus.edu.sg. Fax: (65) 67791691. Edward R. T. Tiekink E-mail: chmtert@nus.edu.sg.

[†] National University of Singapore.

[‡] Institute of Microelectronics.

(1) Sandroff, C. J.; Hwang, D. M.; Chung, W. M. *Phys. Rev. B* **1986**, *33*, 5953.

(2) Sandroff, C. J.; Kelty, S. P.; Hwang, D. M. *J. Chem. Phys.* **1986**, *85*, 5337.

(3) Variano, B. F.; Hwang, D. M.; Sandroff, C. J.; Wiltzius, P.; Jing, T. W.; Ong, N. P. *J. Chem. Phys.* **1987**, *91*, 6455.

(4) Farrugia, L. J.; Lawlor, F. J.; Norman, N. C. *Polyhedron* **1995**, *14*, 311.

(5) Nayal, B. B.; Acharya, H. N.; Mitra, G. B.; Mathur, B. K. *Thin Solid Films* **1983**, *105*, 17.

(6) Pawar, S. H.; Bhosale, P. N.; Uplane, M. D.; Tanhankar, S. *Thin Solid Films* **1983**, *110*, 165.

(7) Black, J.; Conwell, E. M.; Seigle, L.; Spencer, C. W. *J. Phys. Chem. Solids* **1957**, *2*, 240.

(8) Nomura, R.; Kanaya, K.; Matsua, H. *Bull. Chem. Soc. Jpn.* **1989**, *62*, 939.

(9) Peter, L. M. *J. Electroanal. Chem* **1979**, *98*, 49.

(10) Lokhande, C. D. *Mater. Chem. Phys.* **1991**, *27*, 1.

(11) Mane, R. S.; Sankapal, B. R.; Lokhande, C. D. *Mater. Chem. Phys.* **1999**, *60*, 196.

(12) Liao, X. H.; Wang, H.; Zhu, J. J.; Chen, H. Y. *Mater. Res. Bull.* **2001**, *36*, 2339.

(13) Wang, S. Y.; Du, Y. W. *J. Cryst. Growth* **2002**, *236*, 627.

(14) Yu, S. H.; Qian, Y. T.; Shu, L.; Xie, Y.; Yang, L.; Wang, C. S. *Mater. Lett.* **1998**, *35*, 116.

(15) Peng, X. S.; Meng, G. W.; Zhang, J.; Zhao, L. X.; Wang, X. F.; Wang, Y. W.; Zhang, L. D. *J. Phys. D. Appl. Phys.* **2001**, *34*, 3224.

(16) Rincon, M. E.; Sanchez, M.; George, P. J.; Sanchez, A.; Nair, P. K. *J. Solid State Chem.* **1998**, *136*, 167.

(17) Yu, S. H.; Shu, L.; Yang, J.; Zhao, H. H.; Qian, Y. T.; Yu, H. Z. *J. Mater. Res.* **1999**, *14* (11), 4157.

10.1021/cm021813k CCC: $25.00
Published on Web 11/04/2003

fiber-type particles, either in organic solution or by CVD methods. The advantage of the single-source approach is that it is a one-step synthesis compatible with established metallorganic chemical vapor deposition methods in a high vacuum environment. Bismuth compounds that have been investigated recently in this context include tris(benzylthiolato)bismuth,[18] i.e., $Bi(SCH_2Ph)_3$, bismuth tris(methyl-*n*-hexyl-dithiocarbamate), i.e., $Bi(S_2CN(Me)Hex)_3$, and related dithiocarbamate compounds.[19] Solvent thermalysis of these precursors can lead to fiber-type particles which is a distinct advantage compared to the use of commercial Bi_2S_3 powders.

As a contribution in this area, the utility of bismuth tris(O-alkyldithiocarbonate), i.e., $Bi(S_2COR)_3$, more commonly known as bismuth trisxanthate, as a single source precursor in the chemical vapor deposition of bismuth sulfide nanomaterials is investigated in this work. The suitability of the bismuth xanthates in the preparation of Bi_2S_3 has not yet been investigated. Xanthate ligands are known to coordinate metal centers in a variety of coordination modes, e.g. monodentate, bidentate, bridging, etc., giving rise to a rich diversity in their structural motifs.[20] Thermal gravimetric analysis reveals that the bismuth xanthates exhibit a decomposition temperature (<150 °C) lower than that of dithiocarbamate analogues (>250 °C) and, interestingly, the molecular structure of the precursor material appears to influence the nature of the nanoparticles generated from them, in that the thermal decomposition temperature is related to the degree of supramolecular aggregation. The results of this investigation are reported herein.

2. Experimental Section

All reactions were carried out at room temperature. Reagent grade solvents were used without further purification. The starting materials were obtained commercially and were used without purification: anhydrous bismuth(III) chloride (Strem Chemicals Co.), bismuth(III) nitrate pentahydrate (Aldrich), sodium diethyldithiocarbamate trihydrate, bismuth nitrate pentahydrate, and ammonium 1-pyrrolidinecarbodithioic acid (Aldrich Chemical Co). Xanthate ligands, in the form of potassium salts, were generated by the reaction between the precursor alcohol and CS_2 in the presence of KOH. ^1H and $\{^1H\}^{13}C$ NMR spectra were recorded on a Bruker ACF 300 MHz FT NMR spectrometer. Infrared spectra were recorded as KBr disks on an Excalibur Series Bio-Rad Merlin FTS 3000 spectrophotometer. Mass spectra were recorded on a Finnigan TSQ 7000 spectrometer. Elemental analysis was carried out on a Perkin-Elmer PE 2400 CHN and CHNS Elemental Analyzer. Melting points were determined on a BÜCHI B-540 apparatus.

2.1. Synthesis and Characterization of Bismuth(III) Tris(O-alkyldithiocarbonate), $Bi(S_2COR)_3$ for R = Me, Et and ^{i}Pr, and of Bismuth(III) Tris(*N*,*N*-diethyldithiocarbamate, $Bi(S_2CNEt_2)_3$. The compounds $Bi(S_2COMe)_3$,[21] $Bi(S_2COEt)_3$,[22] $Bi(S_2COiPr)_3$,[23] and $Bi(S_2CNEt_2)_3$[24] are known and were prepared using established procedures. Typically, $Bi(NO_3)_3 \cdot 5H_2O$ (2 g, 4.1 mmol) was suspended in aqueous solution (100 mL), and concentrated HCl was added dropwise until a clear solution was obtained. The ligand (12.8 mmol) dissolved in water (20 mL) was added to the clear solution, and the mixture was stirred at room temperature for 30 min. The yellow solid formed was collected by vacuum filtration and the product was recrystallized from chloroform solution.

Bi(S$_2$COMe)$_3$. ^1H NMR: δ 4.25 [s, CH_3]. $\{^1H\}^{13}C$ NMR: δ 226.8 (S_2C); 60.9 (CH_3). Elemental analysis (%) found: C, 13.58; H, 1.69; S, 36.23. Calcd: C, 13.06, H, 1.36; S, 35.40. IR (cm^{-1}): 1205 [ν(C−O)], 1028 [ν(C−S)]. MS: m/z = 422.9 ([Bi(S$_2$COMe)$_2$]$^+$). Yield 71%. mp 130−131 °C.

Bi(S$_2$COEt)$_3$. ^1H NMR: δ 1.53 [3H, t, J 6.8 Hz, CH_3], δ 4.73 [2H, q, J 7.2 Hz, CH_2]. $\{^1H\}^{13}C$ NMR: δ 225.8 (S_2C); 71.3 (CH_2), 13.9 (CH_3). Elemental analysis (%) found: C, 18.76; H, 2.42; S, 34.08. Calcd: C, 18.88, H, 2.62; S, 33.63. IR (cm^{-1}): 1209 [ν(C−O)], 1020 [ν(C−S)]. MS: m/z = 450.8 ([Bi(S$_2$COEt)$_2$]$^+$). Yield 69%. mp 106 °C.

Bi(S$_2$COiPr)$_3$. ^1H NMR: δ 1.49 [6H, d, J 6.0 Hz, CH_3], δ 5.72 [1H, sept, J 6.0 Hz, CH]. $\{^1H\}^{13}C$ NMR: δ 224.9 (S_2C); 80.2 (CH), 21.4 (CH_3). Elemental analysis (%) found: C, 23.50; H, 3.22; S, 31.99. Calcd: C, 23.45; H, 3.42; S, 31.27. IR (cm^{-1}): 1213 [ν(C−O)], 1019 [ν(C−S)]. MS: m/z = 478.9 ([Bi(S$_2$COiPr)$_2$]$^+$). Yield 60%. mp 160−162 °C.

Bi(S$_2$CNEt$_2$)$_3$. ^1H NMR: δ 1.33 [6H, t, J 6.8 Hz, CH_3] and 3.80 [4H, q, J 7.2 Hz, CH_2]. $\{^1H\}^{13}C$ NMR: δ 200.1 (S_2C); 48.3 (CH_2), 12.2 (CH_3). Elemental analysis (%) found: C, 27.57; H, 4.65; N, 6.24; S, 29.99. Calcd: C, 27.53; H, 4.59; N, 6.43; S, 29.44. IR (cm^{-1}): 1481 [ν(C−N)], 984 [ν(C−S)]. MS: m/z = 505.0 ([Bi(S$_2$CNEt$_2$)$_2$]$^+$). Yield 57 %. mp 200−201 °C.

2.2. Synthesis of Chlorobismuth(III) bis(pyrrolinedithiocarbamate), $Bi(S_2CN(CH_2)_4)_2Cl$. $NH_4[S_2CN(CH_2)_4]$ (20.00 mmol, 2.3379 g) dissolved in distilled water (75 mL) was added slowly to a suspension of $BiCl_3$ (6.78 mmol, 2.1376 g) in ethanol (50 mL). The resultant mixture was stirred for 2 h to ensure complete reaction. The bright yellow precipitate was collected using a Buchner funnel and washed with distilled water (3 × 20 mL). The product was then dissolved in $CHCl_3$ (100 mL) and dried over $MgSO_4$. The solvent was later evaporated using a rotary evaporator, and the crude yellow precipitate was recrystallized using an acetonitrile/$CHCl_3$ mixture (1:1 ratio) to yield bright-yellow crystals; these were characterized as a mono-chloroform solvate. Elemental analysis (%) found: C, 22.16; H, 2.92. Calcd: C, 22.37; H, 3.00.

Bi(S$_2$CN(CH$_2$)$_4$)$_2$Cl·CHCl$_3$. ^1H NMR: δ 3.90 (4 H, t, ^3J = 6.83 Hz, NCH_2CH$_2$); δ 2.03 (4 H, m, NCH$_2$CH_2). $\{^1H\}^{13}C$ NMR: δ 196.9 (S_2C); 53.3 (NCH_2CH_2); 25.2 (NCH$_2$CH_2). IR (cm^{-1}): 1479 [ν(C−N)], 991 [ν(C−S)]. MS: m/z = 501 (Bi[$S_2CN(CH_2)_4$]$_2^+$). Yield 62 %. mp 230−232 °C.

2.3. X-ray Crystallographic Analysis of $Bi(S_2CN(CH_2)_4)_2Cl \cdot CHCl_3$. Intensity data for a platelike crystal 0.05 × 0.26 × 0.52 mm were measured at 183 K on a Bruker SMART CCD diffractometer employing Mo Kα radiation so that θ_{max} was 30.0°. Data processing and absorption correction were accomplished with SAINT[25] and SADABS,[26] respectively. The structure was solved by heavy-atom methods[27] and refinement (anisotropic displacement parameters, hydrogen atoms in the riding model approximation, and a weighting scheme of the form $w = 1/[\sigma^2(F_o^2) + (0.0198P)^2 + 2.4228P]$ for $P = (F_o^2 + 2F_c^2)/3$) was on F^2.[28] Crystallographic data and final refinement details are given in Table 1. Some evidence for disorder in the light-atom positions was noted, as judged by rather large thermal motion, but resolution into multiple sites

(18) Boudjouk, P.; Remington, M. P.; Grier, D. G.; Jarabek, B. R.; McCarthy, G. J. *Inorg. Chem.* **1998**, *37*, 3538.
(19) (a) Monteiro, O. C.; Nogueira. H. I. S.; Trindade, T. *Chem. Mater.* **2001**, *13*, 2103. (b) Monteiro, O. C.; Trindade, T.; Park, J.-H.; O'Brien, P. *Chem. Vap. Deposition* **2000**, *6*, 230.
(20) Tiekink, E. R. T.; Winter, G. *Rev. Inorg. Chem.* **1992**, *15*, 161.
(21) Snow, M. R.; Tiekink, E. R. T. *Aust. J. Chem.* **1987**, *40*, 743.
(22) Tiekink, E. R. T. *Main Group Metal Chem.* **1994**, *17*, 727.
(23) Hoskins, B. F.; Tiekink, E. R. T.; Winter, G. *Inorg. Chim. Acta* **1984**, *84*, L13. Hoskins, B. F.; Tiekink, E. R. T.; Winter, G. *Inorg. Chim. Acta* **1985**, *99*, 177.
(24) (a) Howard, J. A.; Russell, D. R.; Scutcher, W. *Acta Crystallogr.* **1975**, *A31*, S141. (b) Raston, C. L.; White, A. H. *J. Chem. Soc., Dalton Trans.* **1976**, 791.
(25) SAINT. Version V5.6. Bruker AXS Inc.: Madison, WI, 2002.
(26) SADABS. (a) Sheldrick, G. M. University of Gottingen: Germany, 2000. (b) Blessing, R. *Acta Crystallogr., Sect. A* **1995**, *51*, 33.
(27) Beurskens, P. T.; Admiraal, G.; Beurskens, G.; Bosman, W. P.; García-Granda, S.; Smits, J. M. M.; Smykalla, C. The DIRDIF Program System; Technical Report of the Crystallography Laboratory, University of Nijmegen, 1992.
(28) Sheldrick, G. M. SHELXL97. Program for crystal structure refinement. University of Göttingen: Germany, 1997.

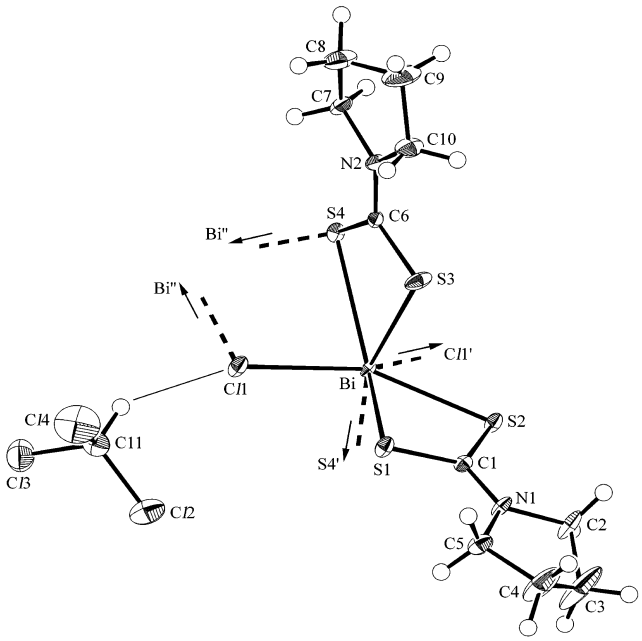

Figure 1. Crystallographic asymmetric unit of $Bi(S_2CN(CH_2)_4)_2Cl{\cdot}CHCl_3$ showing the atomic numbering scheme employed. Selected geometric parameters (Å, °): Bi−Cl1 2.8490(12), Bi−S(1) 2.7263(10), Bi−S(2) 2.7356(10), Bi−S(3) 2.6483(11), Bi−S(4) 2.9924(10), Bi−Cl1′ 2.9466(9), Bi−S4′ 3.1041(10), S1−Bi−S2 65.96(3), S3−Bi−S4 63.45(3), Cl1−Bi−S2 143.43(3), S1−Bi−S4 139.89(3), S3−Bi−S4′ 154.10(3), S4−Bi−S4′ 142.26(1). Singly primed atoms are related by the symmetry operation $0.5 - x$, $0.5 + y$, $0.5 - z$, and the doubly primed atom is related by the symmetry operation $0.5 - x$, $-0.5 + y$, $0.5 - z$.

Table 1. Crystal Data and Refinement Details for $Bi(S_2CN(CH_2)_4)_2Cl{\cdot}CHCl_3$

formula	$C_{11}H_{17}BiCl_4N_2S_4$
M	656.29
crystal system	monoclinic
space group	$P2_1/n$
a/Å	12.7270(6)
b/Å	7.7452(4)
c/Å	21.1854(10)
β/°	100.599(1)
V/Å^3	2052.68(17)
Z	4
μ/mm^{-1}	9.513
D/gm^{-3}	2.124
measured reflections	16366
independent reflections	5955
observed reflections ($I \geq 2\sigma(I)$)	5340
$R(F^2)$ (observed reflections)	0.035
$wR(F^2)$ (all data)	0.088

was not possible. The maximum residual electron density peak of 2.87e Å^{-3} was located in the vicinity of the bismuth atom. Figure 1 was drawn with ORTEP[29] at the 50% probability level, and Figures 2−4 were drawn with the DIAMOND program.[30]

2.4. Thermogravimetric Analysis. The thermogravimetric analyses (TGA) were performed on the above bismuth(III) complexes at 5 °C/min from room temperature to 200−400 °C. Smooth decomposition curves with a well-defined onset temperature were observed for all compounds with the exception of $Bi(S_2CN(CH_2)_4)_2Cl{\cdot}CHCl_3$ owing to the presence of solvent molecules of crystallization in the lattice. The first derivative of the TGA curve confirms that the decomposition occurs at a single step for $Bi(S_2COR)_3$ and $Bi(S_2CNEt)_3$. In the case of $Bi(S_2CN(CH_2)_4)_2Cl{\cdot}CHCl_3$, 10% weight loss at 158 °C might be due to the loss of $CHCl_3$. The decomposition of this compound was observed at 278−320 °C. The observed weight loss of all the compounds matched reasonably well with the calculated value for Bi_2S_3. The TGA results are summarized in Table 2.

Table 2. Summary of the TGA Results

precursor	decomposition temp. (°C)	completion temp. (°C)	weight loss (%)	calculated[a] weight loss (%)
$Bi(S_2COMe)_3$	123	150	50.41	51.53
$Bi(S_2COEt)_3$	110	153	53.25	55.00
$Bi(S_2COiPr)_3$	150	185	58.31	58.16
$Bi(S_2CNEt_2)_3$	219	321	57.87	60.66
$Bi(S_2CN(CH_2)_2)_2Cl{\cdot}CHCl_3$[b]	278	320	55.71	60.80

[a] Calculated assuming formation of Bi_2S_3 as the residue. [b] See text for discussion.

2.5. Preparation of Bi_2S_3 Particulates by the Solvothermal Method. Bi_2S_3 particulates were prepared by solution thermalysis of the bismuth (III) precursors. All reactions were performed in a round-bottom flask fitted to a Liebig condenser under nitrogen atmosphere. A solution of the precursor (0.2 mmol) in ethyleneglycol was refluxed (197 °C) for 2 h using an oil bath. The solution was then left to cool to room temperature. The solid formed was isolated by centrifugation and washed with methanol, and then dispersed in dichloromethane.

2.6. Chemical Vapor Deposition of Bi_2S_3 Thin Films. Film growth experiments were carried out in a low-pressure cold wall reactor by thermal evaporation of the single-source precursor from a boron nitride cup. A dynamic vacuum ($\sim 1 \times 10^{-2}$ Torr) was maintained during the film deposition. The boron nitride cup was maintained at 150−300 °C depending on the evaporation temperature of the precursor used. The substrate used was silicon (100) and its temperature was maintained at 400 °C during growth. The deposition time varied between 5 and 20 min.

2.7. Characterization of the Bi_2S_3 Particulate and Thin Film. X-ray powder diffraction (XRD), X-ray photoelectron spectroscopy (XPS), secondary electron microscopy (SEM), transmission electron microscopy (TEM), and Raman Spectroscopy (RS) were used to characterize the Bi_2S_3 particulates and thin films generated in this study. XRD measurements were performed using a Siemens Instrument operating with Cu Kα radiation (λ = 1.54170 Å) at 40 kV/40 mA and employing a scan rate of 0.03°/s in the 2θ range of 10 to 60°. XPS studies were carried out using Mg Kα radiation (1253.6 eV) on an ESCALAB-220. SEM images were obtained using a JEOL JSM6700 microscope, operating at 10 Amp and 15 KV. TEM was carried out on a Philips 200 microscope, operating at 200 kV. TEM was performed on selected samples obtained from both solvothermal and CVD methods. The Bi_2S_3 thin film removed from the substrates was ultrasonically dispersed in an ethanol solution and then deposited on the carbon grid, whereas the Bi_2S_3 crystals produced by the solvent thermalysis methods were directly deposited on the carbon grid. Raman spectroscopy was performed using a Jobin Yvon T64000 monochromator and confocal collection optics at room temperature. A single-mode 514.5 nm line of an Ar^+ ion laser was used as the light source.

3. Results and Discussion

3.1 Structural Features of the Precursor Compounds. The bismuth thiolate precursors investigated in the present study conform to three distinct structural motifs, depending on the composition of the compound and, in the case of the xanthate compounds, on the nature of the remote organic substituent of the thiolate ligand. Although the crystal structures of $Bi(S_2COR)_3$[21−23]

(29) Johnson, C. K. ORTEP. Report ORNL-5138; Oak Ridge National Laboratory: Oak Ridge, TN, 1976.

(30) DIAMOND, Visual Crystal Structure Information System, Version 2.1e, CRYSTAL IMPACT, Postfach 1251, D-53002 Bonn, Germany, 2002.

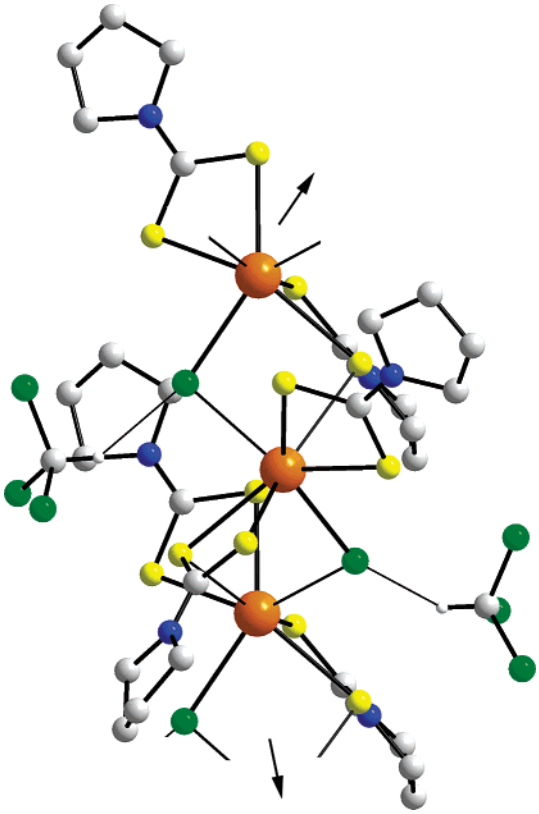

Figure 2. View of the polymeric chain found in the structure of $Bi(S_2CN(CH_2)_4)_2Cl{\cdot}CHCl_3$.

and $Bi(S_2CNEt_2)_3$[24] are known, that of $Bi(S_2CN(CH_2)_4)_2Cl$ is not. The structure of the latter is determined in the present study to be the mono-chloroform solvate. The crystallographic asymmetric unit of $Bi(S_2CN(CH_2)_4)_2Cl{\cdot}CHCl_3$ is illustrated in Figure 1, and selected geometric parameters are given in the figure caption. The bismuth atom is coordinated by two chelating dithiocarbamate ligands and one chloride atom. Immediately apparent from the diagram is the presence of a weak hydrogen bond between the chloride atom bound to bismuth and the hydrogen atom of the solvent $CHCl_3$ molecule of crystallization. The parameters associated with this interaction are Cl···H of 2.59 Å, Cl···C11 of 3.447(6) Å, and an angle of 145° subtended at the H atom. Also apparent from the crystal structure analysis is the fact there is significant intermolecular association operating in the structure. A view of the extended polymeric chain, propagated along the crystallographic *b*-direction by the 2-fold screw symmetry, is shown in Figure 2. The Cl1 and S4 atoms of the asymmetric unit form intermolecular interactions with the same symmetry-related bismuth atom. The Bi−Cl bridge is almost symmetric as seen in the Bi−Cl1 and Bi−Cl1′ bond distances of 2.8490(10) Å and 2.9466(9) Å, respectively and the angle subtended at the bridging chloride atom is 97.14(3)°. In the same way, the S4 bridge is effectively symmetric (2.9924(10) Å and 3.1041(10) Å) with an angle of 90.92(3)° at S4. The bismuth atom is formally seven-coordinate, and contributing to the irregular geometry defined by the Cl_2S_5 donor set about the central atom is the presence of a lone pair of electrons. In the context of the structural diversity noted below, it is interesting to mention that the structures of the closely related mixed dithiocarbamate/halide species, $Bi(S_2CNEt_2)Br$ and $Bi(S_2CNEt_2)_2I$, feature tetrameric and linear polymeric arrays, respectively, each with formally six-coordinate bismuth.[31]

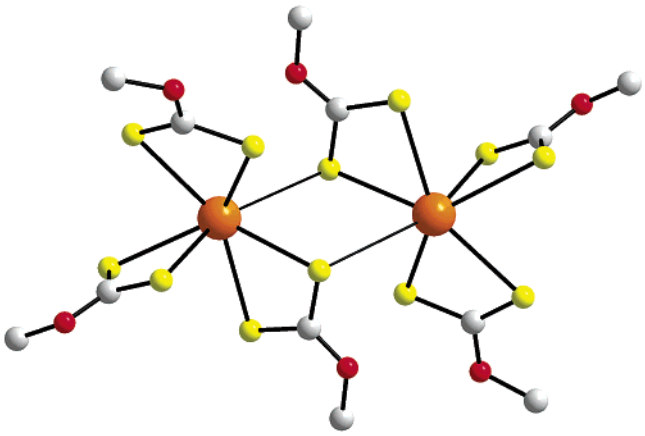

Figure 3. View of the dimeric structure of $Bi(S_2COR)_3$, R = Me and Et. The structure of $Bi(S_2CNEt_2)_3$ is in essential agreement with this motif. Only the alpha carbon and remaining non-hydrogen atoms are shown for clarity.

A representation of the structure of $Bi(S_2COMe)_3$[21] is shown in Figure 3. Here, it can be seen that the bismuth atom is chelated by three xanthate ligands, and monomers associate to form dimeric units. The structure of the ethylxanthate also adopts this motif.[22] However, when the remote R group is changed to an isopropyl group, a profound structural change is apparent. As illustrated in Figure 4, the structure of $Bi(S_2COiPr)_3$ is polymeric,[23] again with seven-coordinate bismuth atoms. Finally, the structure of $Bi(S_2CNEt_2)_3$[24] is dimeric and resembles that shown in Figure 3. No tris-dithiocarbamate structure of bismuth is known to be polymeric, so in order to generate a polymeric array a dithiocarbamate ligand was substituted by a chloride resulting in the formation of polymeric $Bi(S_2CN(CH_2)_4)_2Cl$. In this way, the polymeric xanthate precursor properties may be compared with a polymeric dithiocarbamate analogue. In the ensuing discussion the generation of nanoparticles will be shown to be dependent on the nature of the thiolate ligand (i.e., dithiocarbamate vs xanthate) and upon the nature of the structural motif (i.e., dimeric vs polymeric) at least in the case of the xanthate compounds.

3.2 Preparation of Bi_2S_3 Nanocrystals—Solvothermal Methods. The morphology of the Bi_2S_3 crystals obtained from solvothermal methods was found to be dependent on the solvent used, on the thermalysis temperature, and upon the nature of the precursor employed as alluded to above.[19]

X-ray powder diffraction(XRD) performed on all the powders obtained in this work show that *bismuthinite*, Bi_2S_3, was the crystalline phase present in all samples with diffraction peaks assignable to the orthorhombic Bi_2S_3 structure. No peaks attributable to crystalline bismuth, sulfur, or Bi_2O_3 were observed. Figure 5 shows XRD patterns for several of the Bi_2S_3 powders obtained.

TGA analysis (see Table 2 for summary) reveals that the $Bi(S_2COR)_3$ compounds decompose in one step at

(31) Raston, C. L.; Rowbottom, G. L.; White, A. H. *J. Chem. Soc., Dalton Trans.* **1981**, 1352.

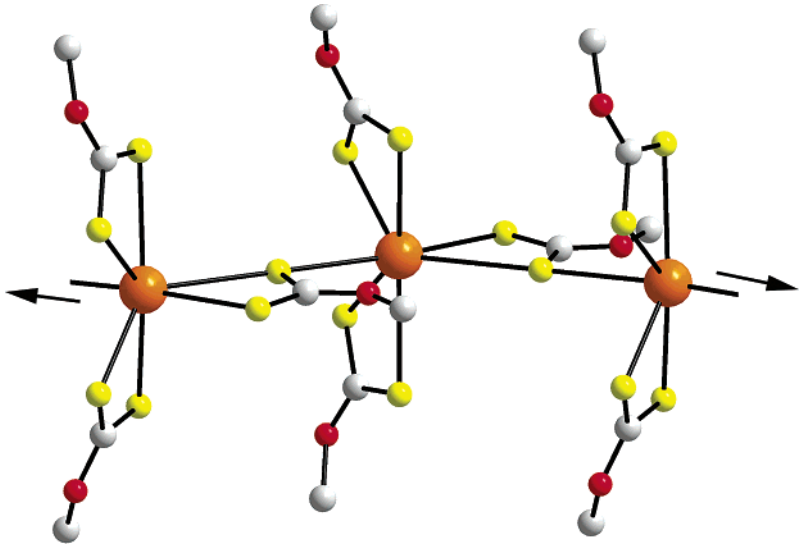

Figure 4. View of the polymeric chain found in the structure of $Bi(S_2COiPr)_3$. Only the alpha carbon and remaining non-hydrogen atoms are shown for clarity.

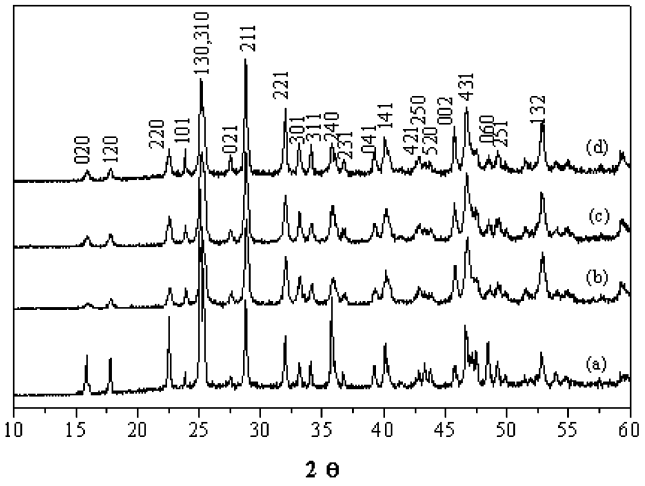

Figure 5. XRD patterns of Bi_2S_3 particulate obtained from solvothermal methods for (a) $Bi(S_2CN(CH_2)_4)_2Cl{\cdot}CHCl_3$, (b) $Bi(S_2COEt)_3$, (c) $Bi(S_2COiPr)_3$, and (d) $Bi(S_2CNEt_2)_3$ single-source precursors.

around 150 °C, whereas the $Bi(S_2CNC_4H_8)_2Cl{\cdot}CHCl_3$ and $Bi(S_2CNEt_2)_3$ compounds require higher decomposition temperatures. Figures 6 and 7 show SEM micrographs of the Bi_2S_3 nanoparticles prepared in ethylene glycol solution at 197 °C. For $Bi(S_2CNC_4H_8)_2Cl{\cdot}CHCl_3$ and $Bi(S_2CNEt_2)_3$, the morphology of the crystals resembles nanotapes, as shown in Figure 6(a) and (b), respectively. The near-transparency of these nanotapes suggests that these are two-dimensional sheetlike structures. Figure 7(a) shows that the crystals recovered from decomposed $Bi(S_2COiPr)_3$ comprise dense nanofibers, with diameters less than 20 nm and lengths exceeding several microns. For $Bi(S_2COiPr)_3$, which is known to adopt a polymeric structure owing to intermolecular bonding as shown in Figure 4, the longest nanofibers were generated as shown in Figure 7(a). For the dimeric precursors $Bi(S_2COR)_3$, R = Et and Me, shorter nanorods were obtained, as observed in Figure 7(b) and (c).

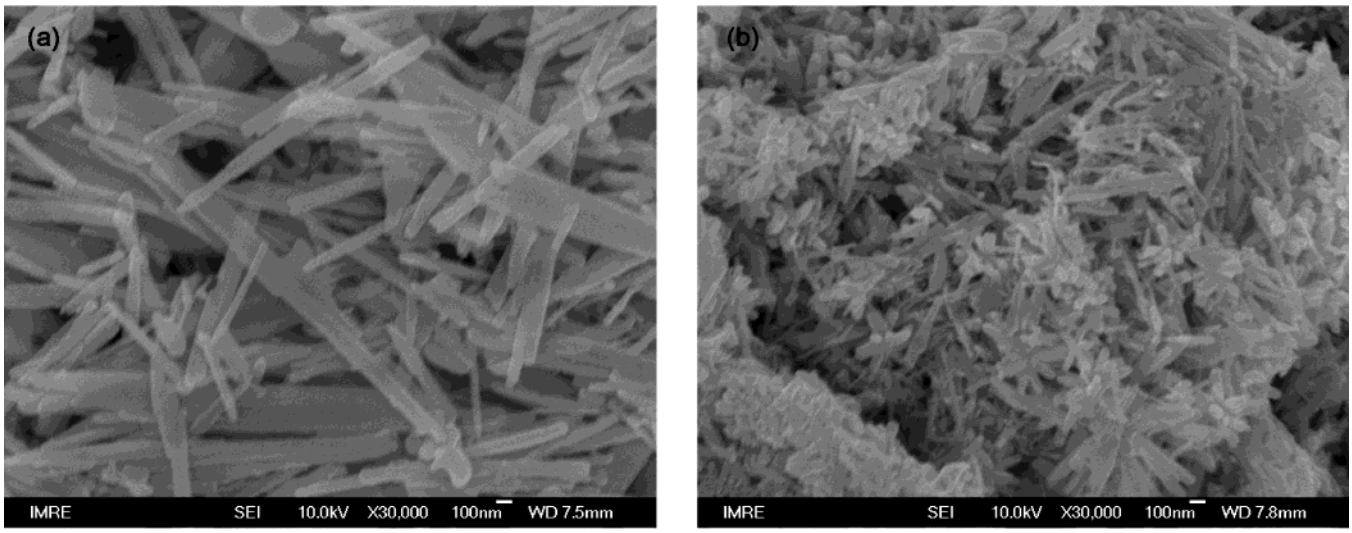

Figure 6. SEM images of the Bi_2S_3 particulate (prepared in ethyleneglycol solution at 197 °C over 2 h) from precursors (a) $Bi(S_2CN(CH_2)_4)_2Cl{\cdot}CHCl_3$ and (b) $Bi(S_2CNEt_2)_3$.

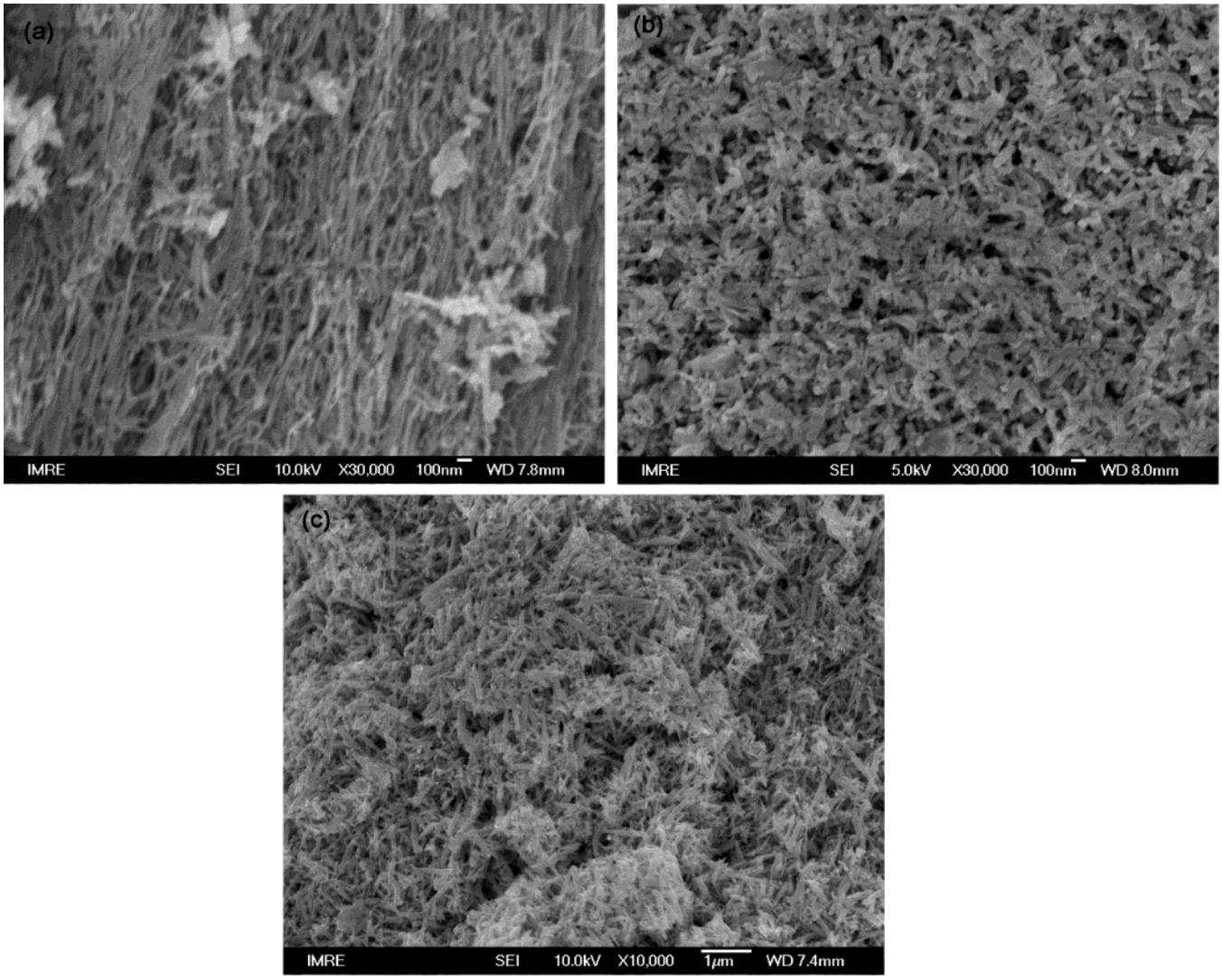

Figure 7. SEM images of the Bi_2S_3 particulate (prepared in ethylene glycol solution at 197 °C over 2 h) from precursors (a) $Bi(S_2COiPr)_3$, (b) $Bi(S_2COEt)_3$, and (c) $Bi(S_2COMe)_3$.

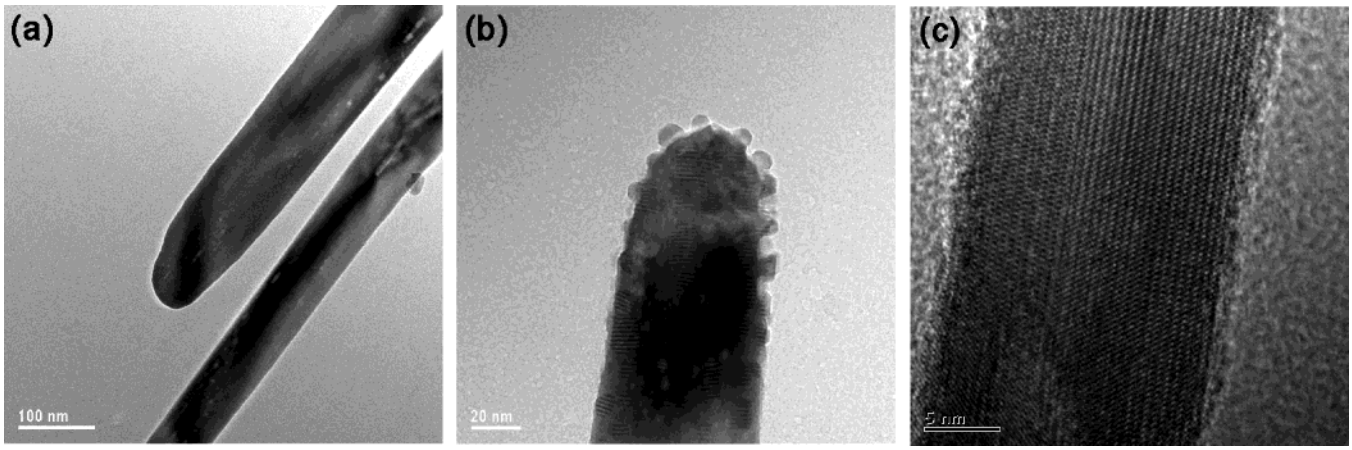

Figure 8. TEM images of Bi_2S_3 rods generated by the solvothermal methods using the precursors $Bi(S_2CN(CH_2)_4)_2Cl{\cdot}CHCl_3$ (a) and (b), and $Bi(S_2CNEt_2)_3$ (c).

High-resolution transmission electron microscopy of Bi_2S_3 particulates is shown in Figure 8. When $Bi(S_2CN(CH_2)_4)_2Cl{\cdot}CHCl_3$ was chosen as the precursor, the diameter of the Bi_2S_3 rod obtained was about 70 nm, as shown in Figure 8(a) and (b). A finer rod with a diameter of 20 nm was obtained using $Bi(S_2CNEt_2)_3$ as the precursor; this is shown in Figure 8(c). In the case of the example shown in Figure 8(b), it was noted that the electron beam, when focused on one region for minutes, induced melting and subsequent recystallization of the Bi_2S_3 phase. This resulted in the formation of "bumps" on the periphery of the rod. Lattice fringes of alternative contrast which are characteristics of the lamellar-type structure in Bi_2S_3 can be observed in 8(c).

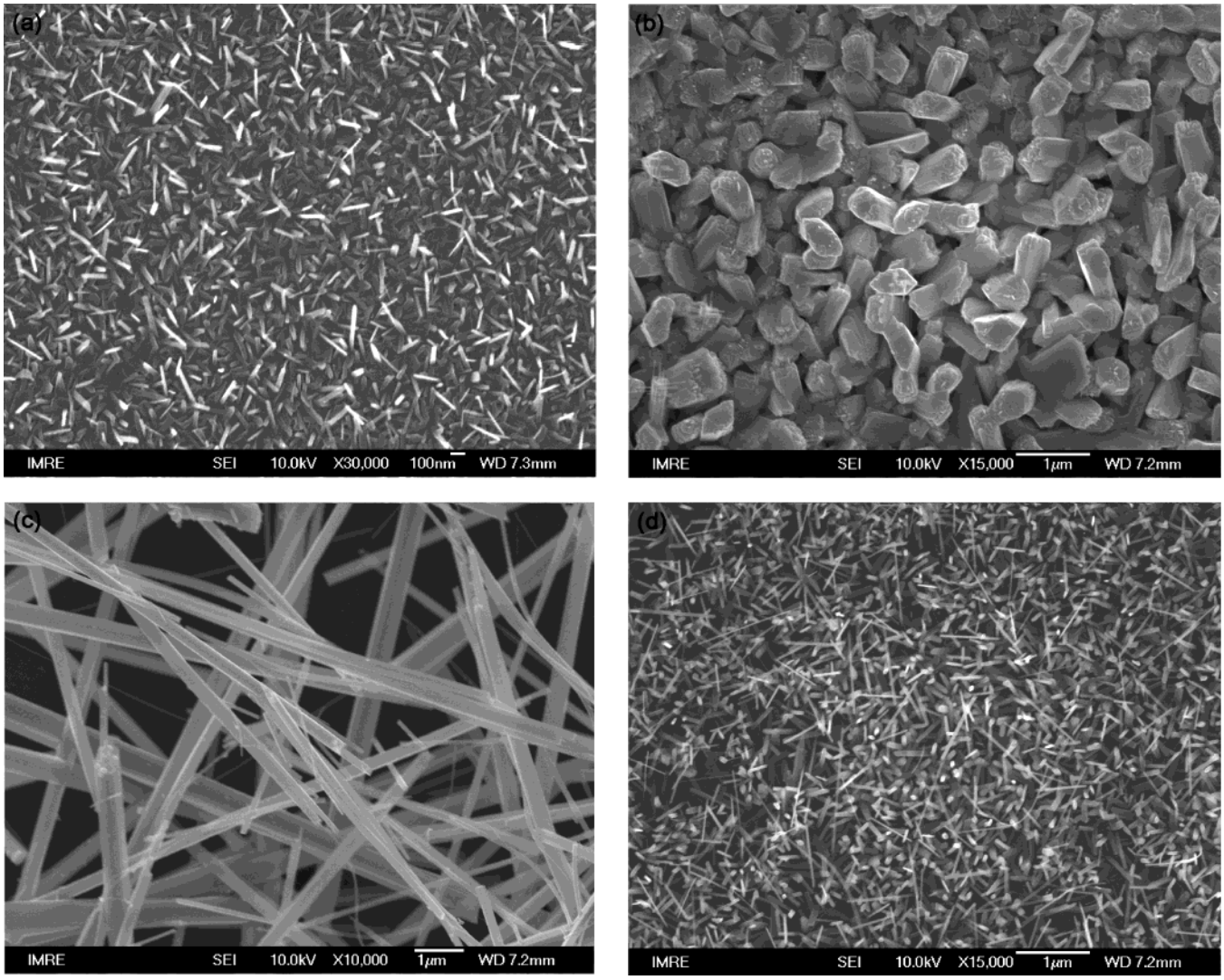

Figure 9. SEM images of Bi_2S_3 thin films generated by CVD using (a) $Bi(S_2COEt)_3$, (b) $Bi(S_2COiPr)_3$, (c) $Bi(S_2CN(CH_2)_4)_2Cl\cdot CHCl_3$, and (d) $Bi(S_2CNEt_2)_3$ as the single-source precursor.

3.3. Chemical Vapor Deposition (CVD) of Bi_2S_3. During CVD, the precursors were evaporated onto the substrate and a heterogeneous reaction resulted in the growth of stoichiometric material. The agglomerization observed for the crystals grown using the solvothermal method was absent and individual rods were observed to nucleate. In almost all cases, the morphology of the Bi_2S_3 thin films obtained was in the form of nanorods that varied only in length. The only exception was when $Bi(S_2COiPr)_3$ was used as the single-source precursor, in this case only submicron sized polycrystals were obtained. Figure 9(a)−(d) shows the SEM images of the Bi_2S_3 thin films grown using different types of precursor.

To investigate the nucleation mechanism of the nanorods, the growth time was shortened to 5 min. As can be seen in Figure 10, aligned nanorods were grown initially suggesting that textured growth on Si(001) was possible. Rod-type morphology observed can be explained by the higher growth rate of Bi_2S_3 along the *c*-axis.[32]

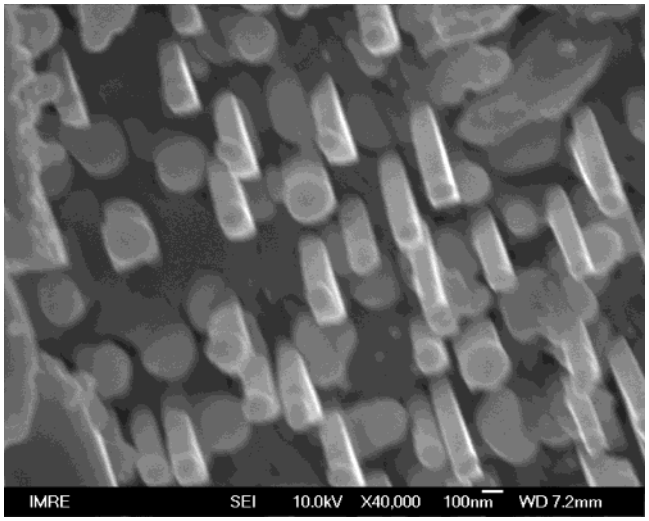

Figure 10. SEM image of aligned Bi_2S_3 nanorods grown following short growth time (5 min) using $Bi(S_2CN(CH_2)_4)_2Cl\cdot CHCl_3$ as the single-source precursor.

XRD was also performed on the CVD-grown samples. As shown in Figure 11(a) and (b), high purity of Bi_2S_3 thin films was obtained only for short deposition times. If the deposition time was increased to longer times,

(32) Rincon, M. E.; Nair, P. K. *Semicond. Sci. Technol.* **1997**, *12*, 467.

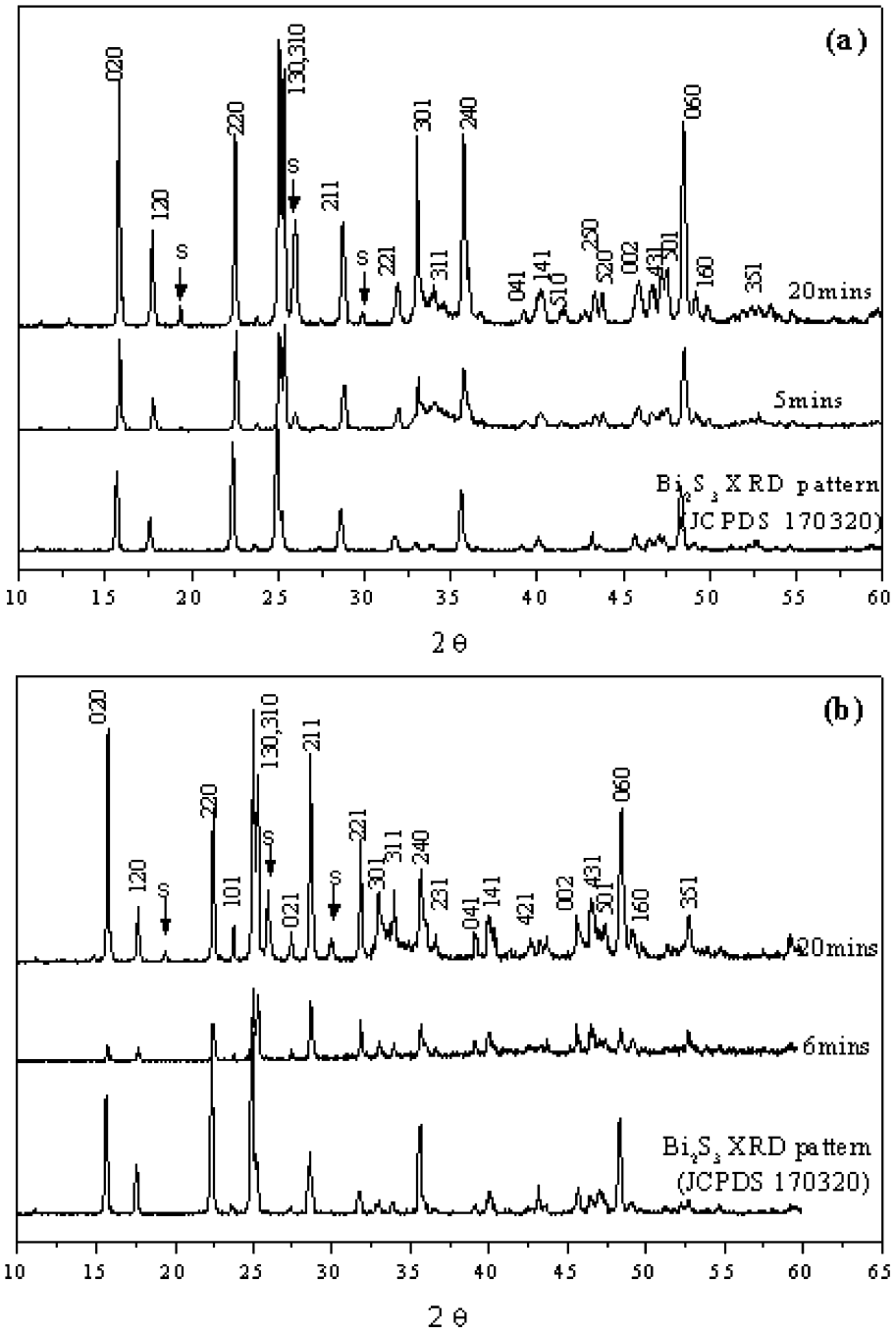

Figure 11. XRD patterns of Bi_2S_3 thin films grown for different intervals using (a) $Bi(S_2COEt)_3$ and (b) $Bi(S_2COiPr)_3$ as the single-source precursors. After 20 min growth, peaks assigned to crystalline sulfur became apparent as indicated.

Table 3. Summary of the Morphology and Diameters of Bi_2S_3 Particulate Obtained from the Solvothermal Method (SM, 2 h) and Chemical Vapor Deposition (CVD, 5 min growth)

precursor	solvothermal method or chemical vapor deposition
$Bi(S_2COMe)_3$	SM: Short rods of 80-nm diameter
$Bi(S_2COEt)_3$	SM: Short rods (av. length 150 nm) that tend to aggregate with diameter 50 nm
	CVD: Needle-shaped rods distributed uniformly across the whole surface of 25-nm diameters
$Bi(S_2COiPr)_3$	SM: Long fibers of 25-nm diameter
	CVD: Micro-sized crystals
$Bi(S_2CNC_4H_8)_2Cl$	SM: Rod-shaped with diameter 100 nm
	CVD: Rod-shaped with lengths of ~500 nm grown in a particular direction and 100-nm diameter
$Bi(S_2CNEt_2)_3$	SM: Short rods (av. length 400 nm) that tend to aggregrate with 100-nm diameter
	CVD: Long rods with lengths of 900 nm to 1~2 μm and diameter 50 nm

crystalline phases corresponding to elemental monoclinic sulfur were observed to segregate on the surface of the thicker films.

The morphologies of the various precursors obtained from solvothermal method and chemical vapor deposition are summarized in Table 3. The diameter of the rods obtained from bismuth xanthate is the smallest regardless of the method employed, an observation demonstrating the importance of the nature of the thiolate employed.

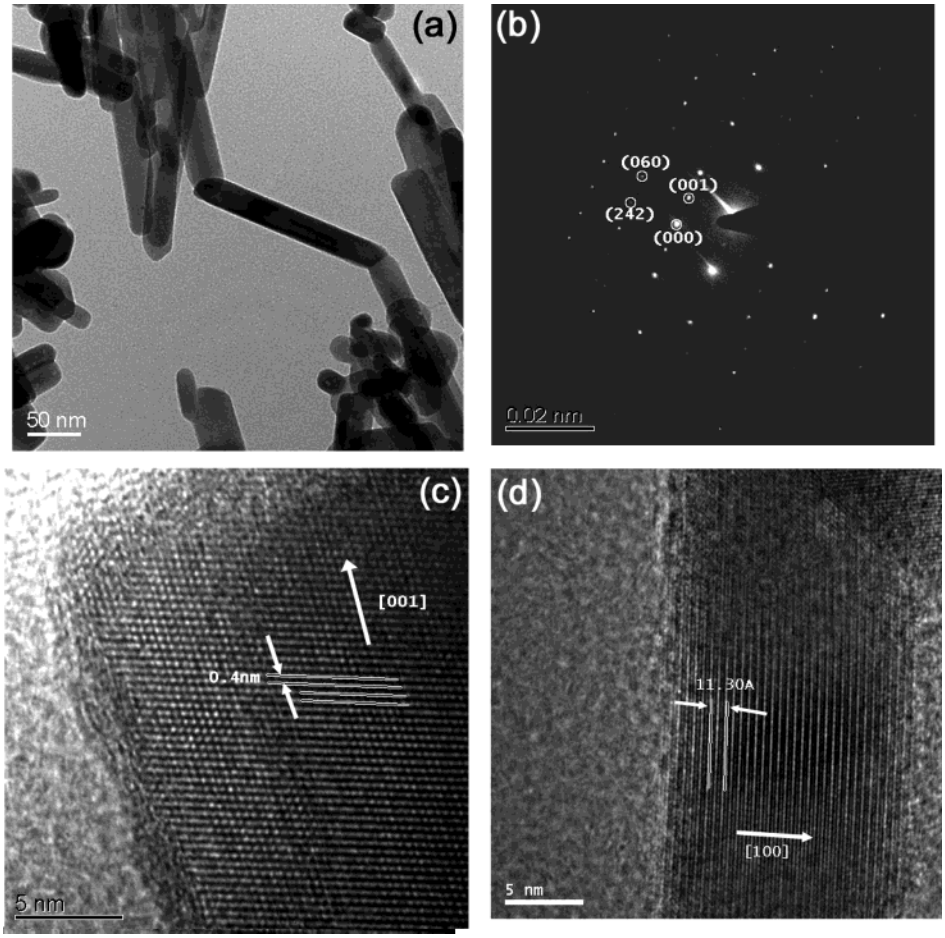

Figure 12. Bi_2S_3 nanorods obtained using $Bi(S_2COEt)_3$ as the single-source precursor: (a) TEM image, (b) electron diffraction pattern, and (c) and (d) HTREM images.

By comparing the XRD pattern of the Bi_2S_3 obtained from solvothermal and CVD methods, it is noticed that the intensities of the diffraction peaks for the (020), (220), and (060) planes for the sample grown by CVD are stronger than that of the sample prepared by solvothermal method. This suggests that there is a textured growth of Bi_2S_3 crystal growth on the (001) face of silicon. The lattice constant of silicon is 5.43 Å, which is close to the dimension of half a bilayer along the *a* or *b* axes of Bi_2S_3 (5.65 Å or 5.57 Å). Our short-time nucleation study revealed that almost aligned growth of nanorods can be achieved initially, with the *c*-axis aligned perpendicular to the substrate (*a* and *b* parallel with the silicon (001) face). We are now extending our study to the UHV environment to achieve the controlled heteroepitaxial deposition of these nanorods on well-characterized silicon.

TEM analysis in Figure 12(a) reveals that the Bi_2S_3 rods obtained are single crystalline. Figure 12(b) shows the electron diffraction pattern. The fringe spacing (0.4 nm) in the (001) direction shown in Figure 12(c) agrees with the *c*-axis of the orthorhombic structure of Bi_2S_3. Therefore the *c*-axis is parallel to the long axis of the fiber. In Figure 12(d), the fringe spacing between two planes is 5.65 Å, which is half of the lattice constant along the (100) direction. The formation of the rod- or fiber-type morphology is ascribed to two reasons. First, the stronger covalent bond between the planes perpendicular to the *c*-axis facilitates higher growth rate along the *c*-axis. The much weaker van der Waals bonding between the planes perpendicular to the *a*-axis limits the growth of the fiber in the horizontal direction and facilitates their cleavage.

XPS was employed to characterize the Bi_2S_3 thin film to evaluate its composition and film purity. The wide scan XPS spectrum is shown as Figure 13. The two strongest peaks at 158.1 and 163.4 eV are assigned to Bi $4f_{7/2}$ and Bi $4f_{5/2}$, respectively. The peak at 225.2 eV corresponds to the S 2*s* transition. Taking into account the atomic sensitivity factor of each element, the ratio of the peak area of Bi 4*f* to S 2*s* was found to be stoichiometric with Bi_2S_3.[12]

Raman spectra of the thin films were recorded between 50 and 400 cm^{-1}. As shown in Figure 14, all the films show five distinct absorptions at 69.8, 169.4, 186.6, 235.8, and 259.6 cm^{-1}. The absorptions at 235.8 and 259.6 cm^{-1} agree with the two Raman bands reported by Wong et al. for a Bi_2S_3 film with a crystal size of 67.5 nm.[12] The origin of the additional peaks at 96.6, 112.6, and 125.2 cm^{-1} observed on the film grown using $Bi(S_2CNC_4H_8)_2Cl$ is not known, but it may be related to surface phonon modes.

4. Conclusions

The growth of single-crystalline bismuth sulfide nanowires from the bismuth trisxanthate precursors has been obtained by both solvent thermalysis and chemical

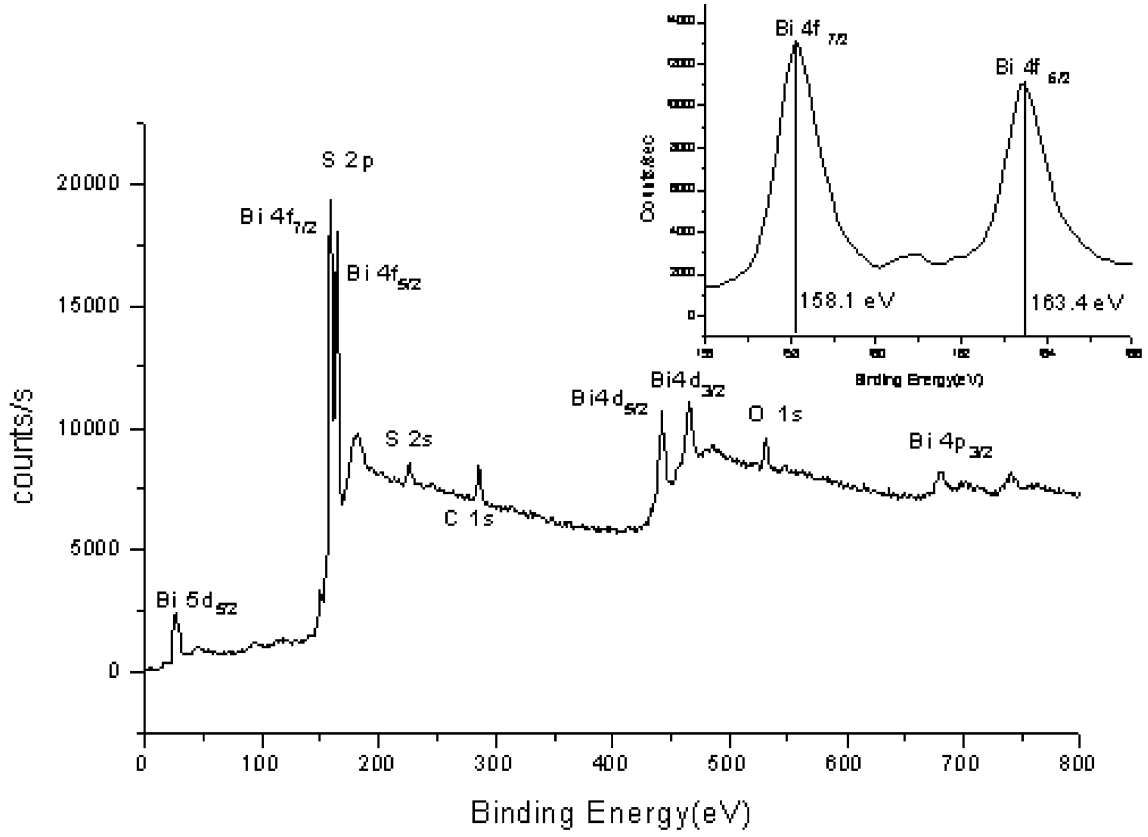

Figure 13. Wide scan XPS spectrum of the Bi_2S_3 generated using the $Bi(S_2COiPr)_3$ precursor.

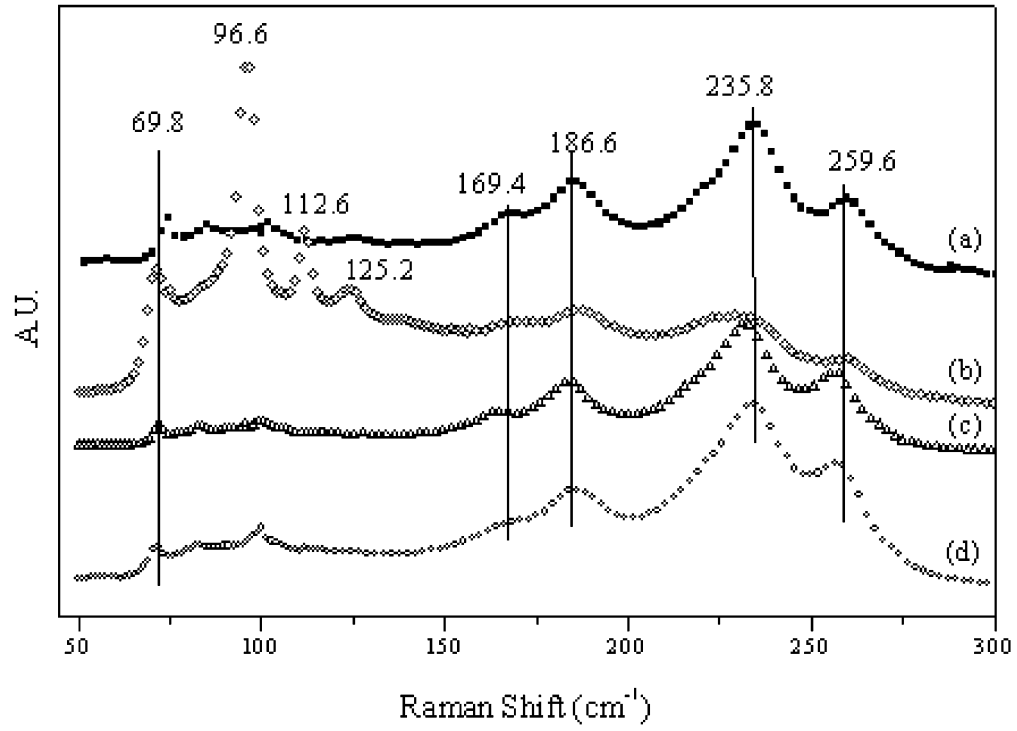

Figure 14. Raman spectra of Bi_2S_3 thin films deposited using (a) $Bi(S_2COiPr)_3$, (b) $Bi(S_2CN(CH_2)_4)_2Cl.CHCl_3$, (c) $Bi(S_2CNEt_2)_3$, and (d) $Bi(S_2COEt)_3$ precursors.

vapor deposition methods. The bismuth xanthates exhibit a lower decomposition temperature (<150 °C) than the dithiocarbamate analogues (>200 °C). It was observed that, generally, precursors adopting the polymeric structural motif in solution decompose at a higher temperature than the precursors with the dimeric motifs. The outcome is that following solvo-thermalysis of these precursors, the polymeric $Bi(S_2COiPr)_3$ gives rise to long Bi_2S_3 nanofibers, whereas dimeric $Bi(S_2COR)_3$ gives rise to nanocrystals. Bi_2S_3 nanowires of various dimensions were obtained invariably by CVD regardless of the bismuth thiolate precursor used.

Acknowledgment. We thank the National University of Singapore and Chartered Semiconductor Manufacturing for a research scholarship awarded to Y.W.K. Support for this research was provided by the National University of Singapore (R-143-000-165-112 and R-143-000-139-112).

Supporting Information Available: Hard copy of crystallographic information file for $Bi(S_2CN(CH_2)_4)_2Cl{\cdot}CHCl_3$ in pdf format (an electronic version may be obtained from chmtert@nus.edu.sg). This material is available free of charge via the Internet at http://pubs.acs.org.

CM021813K